

Energy transfer study in  $\text{GdVO}_4$ :  $\text{Bi}^{3+}$ ,  $\text{Yb}^{3+}$  obtained by microwave-assisted hydrothermal method

Katarzyna Lenczewska, Maciej Ptak, Vitalii Boiko, Karolina Ledwa, Dariusz Hreniak



PII: S0925-8388(20)34756-3

DOI: <https://doi.org/10.1016/j.jallcom.2020.158393>

Reference: JALCOM158393

To appear in: *Journal of Alloys and Compounds*

Received date: 13 November 2020

Revised date: 15 December 2020

Accepted date: 16 December 2020

Please cite this article as: Katarzyna Lenczewska, Maciej Ptak, Vitalii Boiko, Karolina Ledwa and Dariusz Hreniak, Energy transfer study in  $\text{GdVO}_4$ :  $\text{Bi}^{3+}$ ,  $\text{Yb}^{3+}$  obtained by microwave-assisted hydrothermal method, *Journal of Alloys and Compounds*, (2020) doi:<https://doi.org/10.1016/j.jallcom.2020.158393>

This is a PDF file of an article that has undergone enhancements after acceptance, such as the addition of a cover page and metadata, and formatting for readability, but it is not yet the definitive version of record. This version will undergo additional copyediting, typesetting and review before it is published in its final form, but we are providing this version to give early visibility of the article. Please note that, during the production process, errors may be discovered which could affect the content, and all legal disclaimers that apply to the journal pertain.

© 2020 Published by Elsevier.

# Energy transfer study in $\text{GdVO}_4$ : $\text{Bi}^{3+}$ , $\text{Yb}^{3+}$ obtained by microwave-assisted hydrothermal method

Katarzyna Lenczewska<sup>1,\*</sup>, Maciej Ptak<sup>1</sup>, Vitalii Boiko<sup>1,2</sup>, Karolina Ledwa<sup>1</sup>, Dariusz Hreniak<sup>1,\*\*</sup>

<sup>1</sup> Institute of Low Temperature and Structure Research, Polish Academy of Sciences, ul. Okólna 2, PL-50-422 Wrocław, Poland

<sup>2</sup> Institute of Physics of the NAS of Ukraine, Prospect Nauky 46, UA-03028, Kyiv, Ukraine

\* Corresponding author: K.Lenczewska@intibs.pl

\*\* Corresponding author: D.Hreniak@intibs.pl

**Abstract:** Influence of dopants on the structure, morphology and luminescence properties, and in particular the energy transfer mechanism of  $\text{GdVO}_4$  co-doped with  $\text{Bi}^{3+}$  and  $\text{Yb}^{3+}$  ions is discussed. Submicro- and microcrystals were prepared by the microwave-assisted hydrothermal method. Phase purity, size and structure of obtained samples were characterized by the X-ray powder diffraction and the transmission electron microscopy. Luminescence properties were investigated by analyzing photoluminescence and excitation spectra and decay time curves. Intense yellow-green luminescence from  $\text{Bi}^{3+}$  ions in the range of 400-800 nm and the near-infrared emission from  $\text{Yb}^{3+}$  ions about 1000 nm upon an indirect excitation via the ( $\text{O}^{2-}$ - $\text{V}^{5+}$ ) charge transfer state at 266 nm and via the ( $\text{Bi}^{3+}$ - $\text{V}^{5+}$ ) charge transfer state at 330 nm was recorded. No concentration quenching effect was observed in the samples doped with up to 7 mol% of  $\text{Yb}^{3+}$  ions. The near-ultraviolet sensitized near-infrared emission has been explained by the energy transfer from the  $\text{GdVO}_4$  host and  $\text{Bi}^{3+}$  ions to  $\text{Yb}^{3+}$  ions. The energy transfer processes between the host and dopants ions have been characterized in detail. The impact of phonon-assisted processes on the near infrared  $\text{Yb}^{3+}$  emission has been investigated. The obtained spectroscopic characteristics prove that  $\text{GdVO}_4$  co-doped with  $\text{Bi}^{3+}$  and  $\text{Yb}^{3+}$  ions is a promising candidate for use as the phosphor in luminescent concentrators in photovoltaic applications, which can increase the efficiency of silicon-based solar cells.

**Keywords:** vanadates; lanthanides; luminescence; energy transfer; microwave-assisted hydrothermal method

## 1. Introduction

Silicon technology used in photovoltaic applications has limitations related to the upper limit of energy conversion efficiency, which for traditional single-junction solar cells is usually around 30% [1]. Most of the solar energy that hits the cell passes through without being absorbed or becomes heat energy instead. The challenge is to increase this efficiency and reduce energy losses. To enhance the efficiency of silicon-based solar cells the inefficient ultraviolet (UV) photon can be converted to available near-infrared (NIR) photon at around 1  $\mu\text{m}$ , where the Si solar cell exhibits the most efficient spectral response. For this purpose, the use of lanthanide-based luminescent concentrators for solar cells is a very good idea, giving the possibility to convert the chosen energy of sunlight into specific wavelengths [2]. In this scheme, the photoluminescence (both downshifting and downconversion process) takes part in the conversion of high-energy photons into low-energy ones. The downshifting is a one-to-one conversion process, where a photon in the UV-blue is converted into a photon in the red-NIR. In turn, the downconversion processes is more effective because one UV-blue photon is converted at least into two red-NIR photons. Due to the limited absorption capacity of rare earth (RE) ions resulting from their weak absorption, the development of a way of sensitization of their emission

is crucial. Most of the current research carried out in this direction concerns the development of methods of obtaining such materials, which, by co-doping or selecting an appropriate matrix, will absorb and effectively transfer energy to RE ions in a wide range [2,3]. GdVO<sub>4</sub> co-doped with Bi<sup>3+</sup> and Yb<sup>3+</sup> ions was selected as a candidate who could meet the above-mentioned requirements. GdVO<sub>4</sub> itself is an excellent host lattice for a variety of luminescent ions due to its wide range of UV absorption and an efficient energy transfer from [VO<sub>4</sub>]<sup>3-</sup> vanadate groups to activator ions [4,5]. When the host is doped with Bi<sup>3+</sup> ions, the edge of the excitation band shifts toward longer wavelengths with an increase of Bi<sup>3+</sup> content, which can enhance energy transfer efficiency [6]. On the other hand, doping with Yb<sup>3+</sup> ions allows for a near-infrared emission at around 1 μm. This work is in line with the current research trend, which aims to develop suitable phosphors and methods of obtaining them for use as luminescent concentrators. In addition to the obvious condition of spectral matching, one of the ways to enhance conversion efficiency is to maximize the transfer of absorbed solar energy to luminescent centers [3,7].

## 2. Experimental

The powders of GdVO<sub>4</sub>: 1% Bi<sup>3+</sup>, x% Yb<sup>3+</sup> (x = 0, 1, 5, 7 mol%) phosphors and undoped GdVO<sub>4</sub> matrix were prepared by the microwave-assisted hydrothermal method [8]. High purity (99.999%) oxides: Gd<sub>2</sub>O<sub>3</sub>, Yb<sub>2</sub>O<sub>3</sub>, Bi<sub>2</sub>O<sub>3</sub> and a high purity (99.996%) ammonium metavanadate (NH<sub>4</sub>VO<sub>3</sub>) were used as starting reagents for a preparation of the samples. Details of synthesis have been already published in our previous work [9], where we also proved on the example of GdVO<sub>4</sub>: Bi<sup>3+</sup>, Eu<sup>3+</sup> that the maximum content of Bi<sup>3+</sup> ions to avoid their influence on uncontrolled crystal growth is 1 mol% [10]. Briefly, the stoichiometric amounts of oxides were dissolved in ultrapure 65% nitric acid to obtain nitrates. At the same time, the stoichiometric amount of NH<sub>4</sub>VO<sub>3</sub> was dissolved in water. Then, the solution of obtained nitrates was slowly added (one drop per second) to the NH<sub>4</sub>VO<sub>3</sub> solution while stirring vigorously. After the reaction mixture was stirred for another 30 minutes. The homogeneous mixture was transferred to 100 mL Teflon tube and then placed into an autoclave for microwave hydrothermal treatment and allowed to heat for 60 minutes at 180 °C. The obtained precipitate was filtered, washed several times with both distilled water and ethanol. The precipitate was then dried at 60 °C for 24 hours. Finally, the product was calcined at 800 °C for 3 hours in air in order to completely dehydrate the material by removing residual OH groups.

Microwave hydrothermal treatment was carried out in an ERTEC – Magnum II microwave reactor (frequency – 2.45 GHz; power – 600 W). Structural studies of the samples were carried out by means of a X'Pert PRO PANalytical X-ray diffractometer using CuKα radiation (λ = 1.54056 Å). Samples' morphology and microstructure were studied by the use of the Philips CM-20 SuperTwin transmission electron microscope, operating at 160 kV and providing 0.25 nm resolution. Each sample was prepared by grinding a small amount of the sample in a mortar. Then, the ground sample was dispersed in methanol, and a droplet of the suspension was put on the carbon covered microscope grid. Before the measurement, samples were additionally purified using the plasma-cleaner for 1 minute. The Raman spectra were measured using a Renishaw InVia Raman spectrometer equipped with a confocal DM2500 Leica optical microscope, a thermoelectrically cooled CCD as a detector and an argon laser operating at 488 nm. The spectral resolution of Raman spectra was 2 cm<sup>-1</sup>. Absorption spectra were measured with an Agilent Cary 5000 spectrophotometer, employing a spectral bandwidth (SBW) of 0.3 nm in the visible and ultraviolet range and 0.8 nm in the near infrared range. Photoluminescence excitation and emission spectra were measured using an FLS980 Fluorescence Spectrometer from Edinburgh Instruments with an ozone-free 450W Xenon lamp and with detectors:

standard photo- multiplier Hamamatsu R928P and NIR PMT cooled by liquid nitrogen for near infrared emission. Excitation spectra were recorded by using different detector VIS (225-850 nm) and NIR (900-1100 nm). Luminescence decay curves for  $\text{Yb}^{3+}$  ions were recorded with using an FLS980 Fluorescence Spectrometer from Edinburgh Instruments with a 150W Xenon pulsed lamp, whereas luminescence decay curves for  $\text{Bi}^{3+}$  ions were recorded by using a femtosecond laser (Coherent Model “Libra”) emitting 89 fs pulses and pulse energy up to 1 mJ. Conversion Module OPerA) for tuning the laser wavelength between 230 and 2800 nm ( $\lambda_{\text{exc}}$  266 nm). The decay curves were recorded with a Princeton Acton 2500i 0.5 m grating spectrograph coupled with a Hamamatsu C5680 streak camera operating in the 200–1100 nm spectral region with a temporal resolution of 20 ps. All measurements were performed at room temperature (300 K).

### 3. Results and Discussion

Figure 1 presents the X-ray powder diffraction (XRD) patterns of  $\text{GdVO}_4$  samples with 1% (in molar ratio) of  $\text{Bi}^{3+}$  and  $\text{Yb}^{3+}$  doping concentration ranging from 0% to 7% (in molar ratio) obtained directly after the synthesis by the microwave-assisted hydrothermal method (Fig. 1a) and after annealing (Fig. 1b). The necessary calcination process aimed to remove from the material the remains of hydroxyl (OH) groups, including those from the first coordination sphere of dopant ions, which are one of the main reasons for quenching the luminescence of rare-earth ions through a process of multiphonon relaxation [11]. As shown in the further part of the work by the luminescence measurement, the removal of internally bonded OH groups surrounding lanthanide ions is finally completed after heat treatment at 800 °C. The XRD patterns for all samples clearly show the presence of the tetragonal zircon-type  $\text{GdVO}_4$  crystal structure corresponding to the PDF [00-017-0260] card. As can be seen on a zoom of the (200) diffraction peak in Figure 1a', the increase of  $\text{Yb}^{3+}$  concentration in the sample causes a shift of the diffraction peaks to a higher angle side. This result means that the lattice parameters slightly decreased after co-doping with  $\text{Yb}^{3+}$  ions. The lattice contraction effect can be due to the smaller  $\text{Yb}^{3+}$  ions doping, which introduced in the place of the  $\text{Gd}^{3+}$  ion [12,13]. On the other hand, this lattice contraction can be also due to a size effect [14]. It is observed also that with increasing of  $\text{Yb}^{3+}$  ions a size of crystallites decreases, what is clearly visible in the TEM photos in Figure 2 a, b, c and increases after annealing process (Fig. 2 A, B, C). Therefore, two factors can influence on the lattice contraction effect. After annealing at 800 °C, the lattice contraction effect is also noticed but much smaller (Fig. 1b') than for as-prepared samples. An influence of particle size on lattice parameters has been also analysed in other oxide materials like  $\text{GdVO}_4:\text{Eu}^{3+}$  [15] and  $\text{CoFe}_2\text{O}_4$  [16], there was observed that a lattice parameters increase with increasing of particle size after annealing. The annealing process results in a decrease in the defects, internal strains due to coalescence of crystallites, which in turns results in an increase in the average size of the nanoparticles. Therefore during annealing in the air atmosphere, the lattice contraction effect becomes smaller.

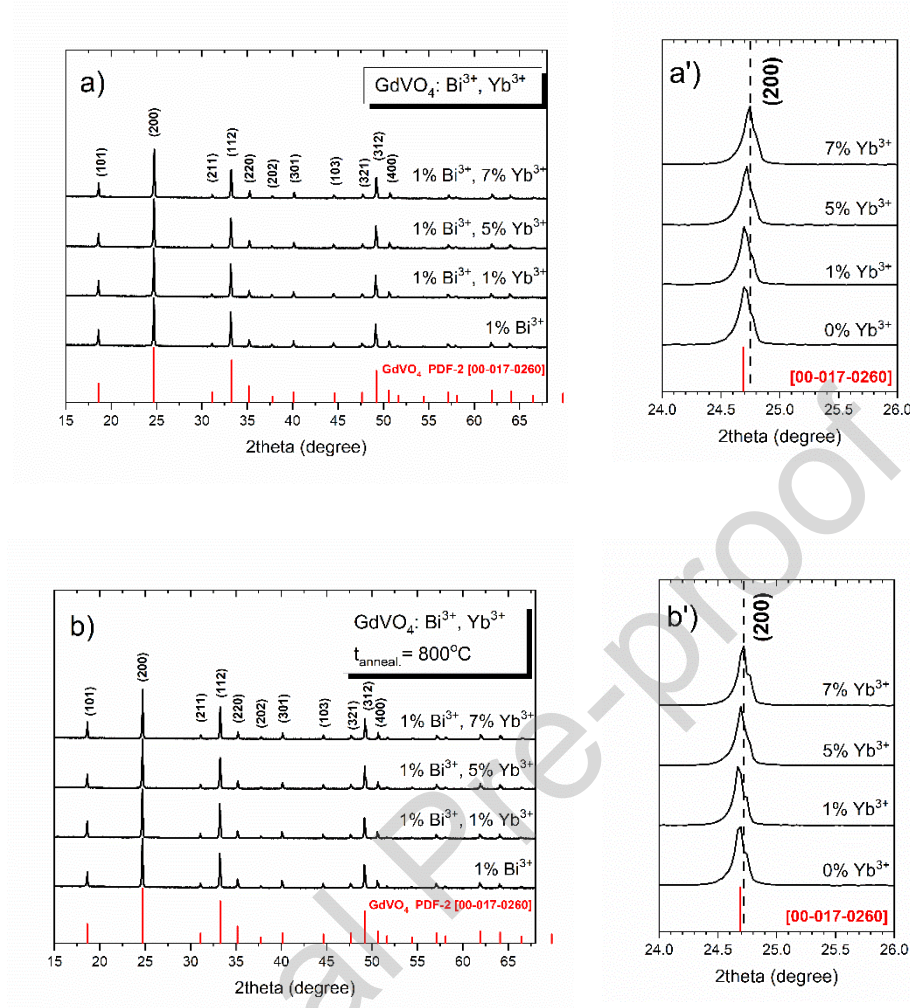


**Figure 1.** XRD patterns of  $\text{GdVO}_4: 1\% \text{Bi}^{3+}, x\% \text{Yb}^{3+}$  ( $x = 0, 1, 5, 7$ ) obtained directly after the synthesis (a) and after annealing at  $800\text{ }^\circ\text{C}$  (b) and a zoom of the (200) diffraction peak of  $\text{GdVO}_4$  pattern and samples with the various concentrations of  $\text{Yb}^{3+}$  directly after the synthesis (a') and after annealing at  $800\text{ }^\circ\text{C}$  (b').

Transmission electron microscopy (TEM) images in Fig. 2 present the morphology of the obtained samples. The shape and size of particles change significantly after annealing at  $800\text{ }^\circ\text{C}$ . The size and in particular the shape of the particles is more spherical without clearly exposed walls, which can be seen in the as-prepared particles. Increasing the size of the crystallites with the with annealing temperature is a result of the Oswald's ripening process [17]. The change in grain size depending on the annealing temperature and its significant effect on the luminescence properties has been observed and described earlier for  $\text{GdVO}_4$  co-doped with  $\text{Bi}^{3+}$  and  $\text{Eu}^{3+}$  ions, but synthesized by modified Pechini's method [6]. In addition, it can be seen from the TEM images that the grain size decreases with increasing of  $\text{Yb}^{3+}$  ions concentration from 1% to 7% for samples obtained directly after the synthesis (Fig. 2 a, b, c) and remains almost unchanged for the samples annealed at  $800\text{ }^\circ\text{C}$  (Fig. 2 A, B, C). This helps to clarify previous doubts as to the reasons leading to the observed the lattice contraction effect. By analyzing the peak shift (200) before and after annealing (Fig. 1a' and b') and comparing it with the corresponding TEM images, it can be concluded that in the studied case the effect of doping with heavier and smaller ions has a weaker effect on the network parameter than the mentioned size effect related to the surface structure. This effect has been observed and analyzed in

our earlier work about  $\text{GdVO}_4$  co-doped with  $\text{Bi}^{3+}$  and  $\text{Yb}^{3+}$  ions but synthesized by modified Pechini's method, which yields grains much more heterogeneous and agglomerated [12].

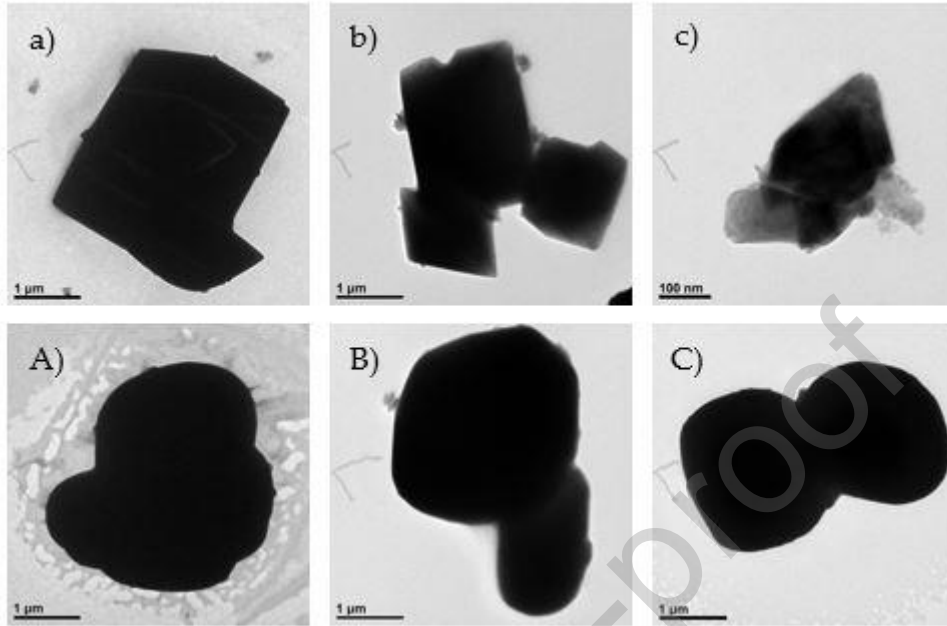
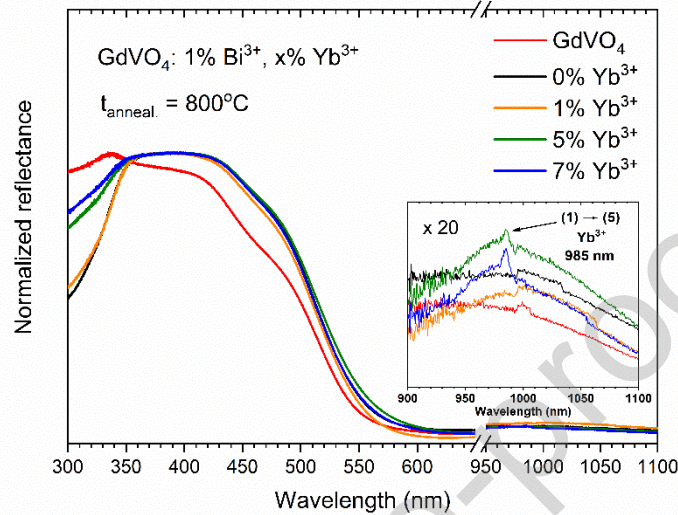


**Figure 2.** TEM images of the samples obtained directly after the synthesis: (a)  $\text{GdVO}_4$ : 1%  $\text{Bi}^{3+}$ , 1%  $\text{Yb}^{3+}$ , (b)  $\text{GdVO}_4$ : 1%  $\text{Bi}^{3+}$ , 5%  $\text{Yb}^{3+}$ , (c)  $\text{GdVO}_4$ : 1%  $\text{Bi}^{3+}$ , 7%  $\text{Yb}^{3+}$  and after annealing at 800 °C (A), (B) and (C), respectively.

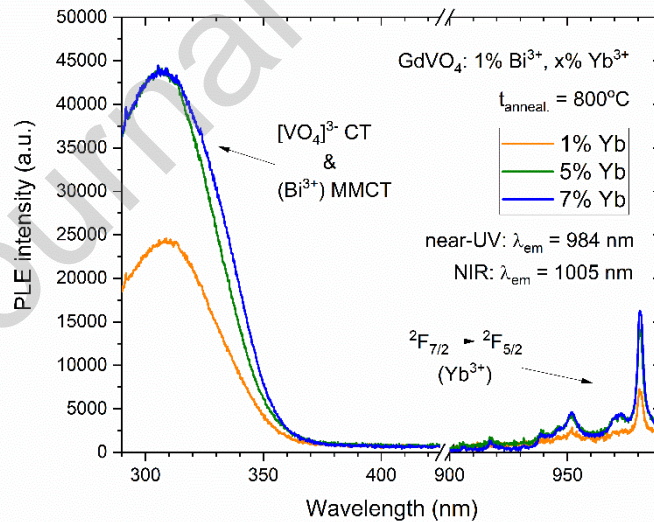
The UV-visible-NIR diffuse reflectance spectra of pure and co-doped  $\text{GdVO}_4$  annealed at 800 °C are presented in Figure 3. The strong absorption band below 600 nm of the spectrum is ascribed to the host absorption, where for pure  $\text{GdVO}_4$  this band can be primarily ascribed to the charge transfer (CT) transition from  $\text{O}^{2-}$  to different levels of  $\text{V}^{5+}$  in the tetrahedral  $[\text{VO}_4]^{3-}$  group and for  $\text{GdVO}_4$  doped with 1%  $\text{Bi}^{3+}$  ions it can be also ascribed to the metal-to-metal charge transfer (MMCT) transition from  $\text{Bi}^{3+}$  to  $\text{V}^{5+}$  [18,19]. Whereas in the NIR range (inset), it can be seen the absorption peak at around 985 nm, which is co-called a zero phonon line of the  $\text{Yb}^{3+}$  ion. The zero phonon line is the transition from the lowest Stark level of the  ${}^2\text{F}_{7/2}$  (1) ground state to the lowest Stark level of the  ${}^2\text{F}_{5/2}$  (5) excited state of  $\text{Yb}^{3+}$  ion. The position of the absorption peak is the same as in the  $\text{Yb}^{3+}$  doped  $\text{GdVO}_4$  crystal [20]. This absorption transition is visible only for the highest  $\text{Yb}^{3+}$  concentrations (5% and 7%) in the studied samples. It can be seen also that the absorption edge is shifted in direction of the longer wavelengths for samples doped with  $\text{Bi}^{3+}$  ions. This red shift of the absorption edge results from the fact that  $\text{Bi}^{3+}$  ions contribute to narrowing of the band gap [21,22]. In addition, the studied materials are optically transparent in the red range. Since the host absorption is very strong compared to the absorption of  $\text{Yb}^{3+}$  ions, an excitation of dopant ions indirectly e.g. using wavelength in the near-UV range is possible due to this property of the host.

Figure 4 shows the near-UV and NIR part of the range of the photoluminescence excitation (PLE) spectra depend on the  $\text{Yb}^{3+}$  concentration when monitoring the emission from  $\text{Yb}^{3+}$  ions at 984 nm in the near-UV range and at 1005 nm in the NIR range. The band in the range 290-370 nm consists of two CT bands:  $[\text{VO}_4]^{3-}$  CT band and  $(\text{Bi}^{3+}-\text{V}^{5+})$  MMCT band, while the group of bands in the range of 900-990 nm is the  $\text{Yb}^{3+}$  absorption band corresponding to the  ${}^2\text{F}_{7/2} \rightarrow {}^2\text{F}_{5/2}$  transition. A shape of the absorption bands does not change with increasing of  $\text{Yb}^{3+}$  ions concentration. The observed PLE spectra prove that the indirect excitation of  $\text{Yb}^{3+}$  ions is possible. Comparing spectra from Figures 3 and 4 it can be seen that the range of observed absorption bands does not coincide with the recorded

excitation spectra. This shows that the optically active area is below 370 nm. On the other hand, the area in the range of 370-600 nm, which does not contribute to luminescence, it may be associated with a distortion of the structure [22] or defects of the surface, which are related to a change in a morphology of the host [23] or the presence of a trace amount of passive impurities [24,25]. These effects may be responsible also for the dark-yellow color of powders.



**Figure 3.** UV-visible-NIR diffuse reflectance spectra of pure and  $\text{Bi}^{3+}/\text{Yb}^{3+}$  co-doped  $\text{GdVO}_4$  annealed at 800 °C.



**Figure 4.** Photoluminescence excitation (PLE) spectra of  $\text{Yb}^{3+}$  ions in  $\text{Bi}^{3+}/\text{Yb}^{3+}$  co-doped  $\text{GdVO}_4$  annealed at 800 °C upon  $\lambda_{\text{em}} = 984$  nm - in the near-UV range and upon  $\lambda_{\text{em}} = 1005$  nm - in the NIR range.

Raman spectra of pure and co-doped  $\text{GdVO}_4$  obtained directly after the synthesis as well as annealed at 800 °C are presented in Figure 5. In Figure 5a there are seen internal (higher-frequencies) and external (lowest-frequencies) vibrational modes of the crystalline lattice in the  $\text{GdVO}_4$  compound. The internal vibrational modes correspond to internal vibrations of the  $[\text{VO}_4]^{3-}$  tetrahedra and the external vibrational modes comprise translations and librations of the  $[\text{VO}_4]^{3-}$  tetrahedra as rigid units

against the rare-earth ions [26]. Internal modes consist symmetric  $\nu_s(\text{VO}_4)$  and asymmetric  $\nu_{as}(\text{VO}_4)$  stretching vibration modes in the range of 800-900  $\text{cm}^{-1}$  and asymmetric  $\delta_{as}(\text{VO}_4)$  and symmetric  $\delta_s(\text{VO}_4)$  bending modes, which are typically present in the range of 300-500  $\text{cm}^{-1}$ , whereas the external vibrational modes four peaks are observed in the range of 100-300  $\text{cm}^{-1}$  [27,28]. The most intense peak at 882  $\text{cm}^{-1}$  corresponds to a maximum phonon energy in the  $\text{GdVO}_4$  compound. This value is similar to that in the  $\text{GdVO}_4$  crystal (884  $\text{cm}^{-1}$ ) [29] and obtained in our earlier work about  $\text{GdVO}_4$  co-doped with  $\text{Bi}^{3+}$  and  $\text{Yb}^{3+}$  ions (882  $\text{cm}^{-1}$ ) synthesized by modified Pechini's method [12]. Raman spectra presented for samples annealed at 800 °C in Figure 5b contain additional peaks that have been identified as vibrational modes coming from  $\text{V}_2\text{O}_5$  impurity [30,31]. These additional peaks are not observed in Raman spectra for samples directly after synthesis. It can mean that amorphous  $\text{V}_2\text{O}_5$  impurity has undergone a crystallization process after annealing at 800 °C, and therefore, becomes observable in Raman spectra as clear peaks. The presence of this impurity explains also yellowish color of powders after annealing ( $\text{V}_2\text{O}_5$  crystals have dark-yellow color). This impurity is a separate phase in the doped  $\text{GdVO}_4$  compound obtained by synthesis and occurs in a negligible amount that is undetectable on XRD patterns of samples. This allows for the use of the synthesized material for further spectroscopic studies.

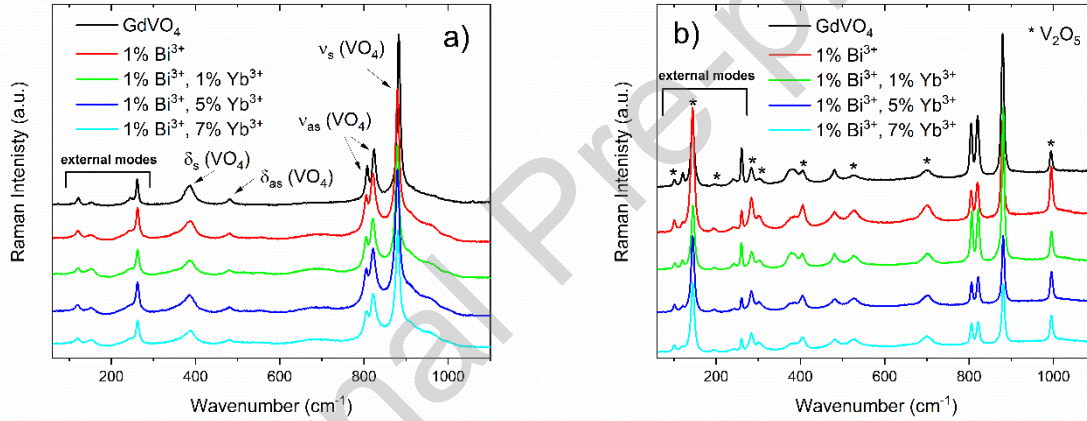


**Figure 5.** Raman spectra of  $\text{GdVO}_4$  host,  $\text{GdVO}_4$ : 1%  $\text{Bi}^{3+}$  and  $\text{GdVO}_4$ : 1%  $\text{Bi}^{3+}$ ,  $x\%$   $\text{Yb}^{3+}$  ( $x = 0, 1, 5, 7$ ) obtained directly after the synthesis (a) and after annealing at 800 °C (b). The asterisks mark  $\text{V}_2\text{O}_5$  impurity (see text).

In Figure 6 the reflectance, excitation and emission spectra of the 1%  $\text{Bi}^{3+}$  doped  $\text{GdVO}_4$  and co-doped with the highest concentration (7%) of the  $\text{Yb}^{3+}$  ions samples annealed at 800 °C have been compared. All spectra have been normalized to the maximum of their band. It can be seen that reflectance spectra and excitation spectra in the UV-visible range for both samples are very similar. The identical shape of the excitation spectra for both samples indicates that the same energy range is responsible for the emission of both  $\text{Bi}^{3+}$  and  $\text{Yb}^{3+}$  ions. This, in turn, may mean that the  $\text{Yb}^{3+}$  emission is an effect of energy transfer from the  $\text{Bi}^{3+}$  ions. Upon 330 nm irradiation, exciting both the ( $\text{Bi}^{3+}-\text{V}^{5+}$ ) MMCT state and also partially the ( $\text{O}^{2-}-\text{V}^{5+}$ ) CT one (a strong overlap of both bands), the  $\text{GdVO}_4$  sample doped with 1%  $\text{Bi}^{3+}$  shows an intensity yellow-green emission which is represented by a broad band in the range of 400-800 nm with a maximum at 575 nm. This band is associated with the MMCT  $\rightarrow {}^1\text{S}_0$  transition of the  $\text{Bi}^{3+}$  ion. In the case of the sample 1%  $\text{Bi}^{3+}$ / 7%  $\text{Yb}^{3+}$  co-doped  $\text{GdVO}_4$ , apart the emission from the  $\text{Bi}^{3+}$  ions, the emission in the near-infrared range from the  $\text{Yb}^{3+}$  ions has been also observed. The specific band in the NIR range (930-1070 nm) with a maximum at 984 nm (a zero phonon line) is well known and interpreted as the  ${}^2\text{F}_{5/2} \rightarrow {}^2\text{F}_{7/2}$  transition of the  $\text{Yb}^{3+}$  ion. The obtained

results show that under indirect excitation (330 nm) the investigated co-doped material exhibits a visible and NIR emission as an effect of energy transfer from  $\text{Bi}^{3+}$  ions to  $\text{Yb}^{3+}$  ions.

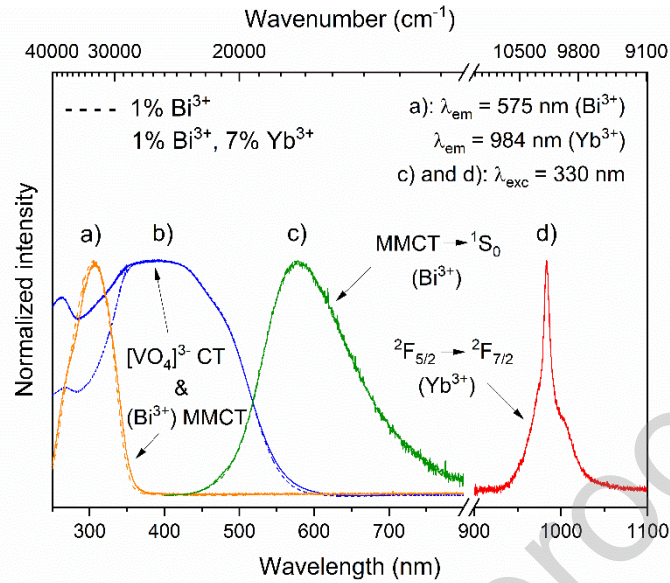


**Figure 6.** Excitation spectra at  $\lambda_{em} = 575$  nm ( $\text{Bi}^{3+}$ ) and  $\lambda_{em} = 984$  nm ( $\text{Yb}^{3+}$ ) (a), reflectance spectra (b), emission spectra ( $\lambda_{exc} = 330$  nm) of  $\text{Bi}^{3+}$  (c) and  $\text{Yb}^{3+}$  (d) of  $\text{Bi}^{3+}$  doped  $\text{GdVO}_4$  (dash line) and  $\text{Bi}^{3+}/\text{Yb}^{3+}$  co-doped  $\text{GdVO}_4$  (solid line) annealed at  $800^\circ\text{C}$ , respectively.

The energy transfer process between  $\text{Bi}^{3+}$  and  $\text{Yb}^{3+}$  ions is very well visible in Figure 7. Upon an excitation both in the UV and near-UV range, the emission intensity from  $\text{Bi}^{3+}$  ions decreases with the increasing concentration of  $\text{Yb}^{3+}$  ions. It confirms that a part of energy from excited  $\text{Bi}^{3+}$  ions can be transferred to the  $\text{Yb}^{3+}$  ions leading to the NIR luminescence with the simultaneous possibility of modulating the intensity of both bands by selecting the appropriate level of doping with  $\text{Yb}^{3+}$  ions. Additionally, the  $\text{Yb}^{3+}$  luminescence quenching effect for the concentration of  $\text{Yb}^{3+}$  ions in the range of 1% - 7% at both 266 nm and 330 nm excitation is not observed.

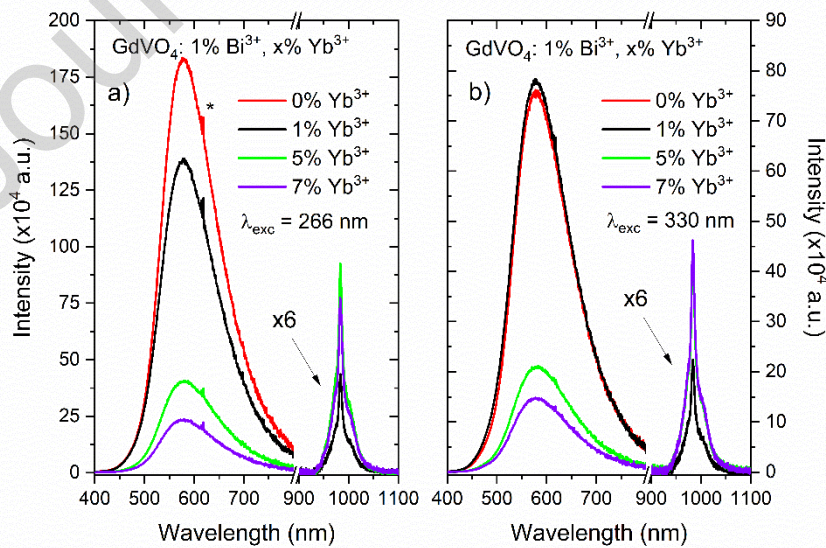


**Figure 7.** Photoluminescence emission spectra of  $\text{GdVO}_4: 1\% \text{Bi}^{3+}, x\% \text{Yb}^{3+}$  ( $x = 0, 1, 5, 7$ ) annealed at  $800^\circ\text{C}$  upon excitation  $\lambda_{exc} = 266$  nm (a) and  $\lambda_{exc} = 330$  nm (b). \*Artefacts from the xenon lamp.

In Figure 8, the  $\text{Yb}^{3+}$  luminescence and NIR excitation spectra (a, b) plotted and Raman spectrum (c) for the sample with the highest concentration of the  $\text{Yb}^{3+}$  ions at room temperature are reported. Dashed lines mark the expected position of Raman modes originated from the  $\text{GdVO}_4$ : 1%  $\text{Bi}^{3+}$ , 7%  $\text{Yb}^{3+}$  sample (see Figure 5a and 5b). The shown spectra were adjusted to the same energy scale, by taking the origin of the absorption and the emission at the zero phonon line, in coincidence with the Rayleigh line of the laser (488 nm) used to record the Raman spectra. By rotating the absorption spectrum around the origin of  $180^\circ$ , we get a direct comparison with both emission and Raman spectra, which are then drawn to the lowest frequency side [32]. Keeping in mind the hypothesis that the Raman spectrum should reflect vibronic structures accompanying each pure electronic transition [33], this simple experimental method helps to distinguish between electronic and vibronic transitions. Absorption spectra recorded at room temperature in Figure 8 are broad which testifies to their vibrational nature caused by electron-phonon coupling and what confirm overlapped absorption peaks seen in the excitation spectrum with two vibronic bands which appear below  $200\text{ cm}^{-1}$  (Fig. 8b and c). This is a typical phenomenon for  $\text{Yb}^{3+}$  doped orthovanadates [34,35] and for other oxides compounds e.g. orthosilicates [36]. This coupling manifests itself even in the  $\text{Yb}^{3+}$  doped  $\text{GdVO}_4$  spectrum recorded at 25 K [37] and also in the  $\text{Yb}^{3+}$  doped  $\text{YVO}_4$  spectrum recorded at 4.2 K [35]. The vibrational structure accompanying the electronic transitions makes it difficult to identify the crystal field components of the  $\text{Yb}^{3+}$  ion electronic levels. In addition, the broadband emission and the inability to distinguish individual electron transitions in the powder sample also results from the crystal anisotropy because the crystals of  $\text{GdVO}_4$  form optically uniaxial crystals analogously to  $\text{YVO}_4$  crystals [35]. When comparing the excitation and Raman spectra presented depending on the concentration of  $\text{Yb}^{3+}$  dopant in the samples in the Figures 4 and 5, it can be seen that the electron-vibronic excitation spectra do not depend essentially on the concentration of  $\text{Yb}^{3+}$  and the size of the crystallite grains.

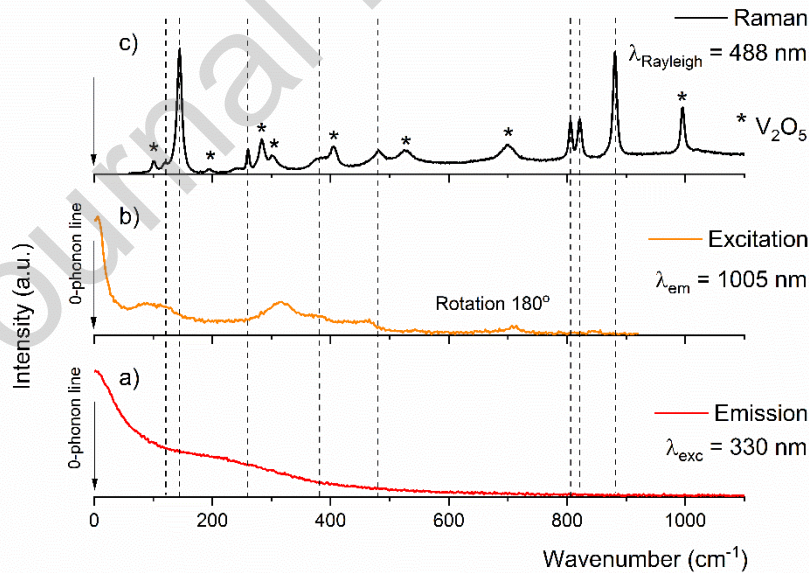


**Figure 8.** Comparison of  $\text{Yb}^{3+}$  emission (a),  $\text{Yb}^{3+}$  NIR excitation (b) and Raman spectrum (c) showing electronic and vibronic structure  $\text{Yb}^{3+}$  ions in the  $\text{GdVO}_4$ : 1%  $\text{Bi}^{3+}$ , 7%  $\text{Yb}^{3+}$  powders annealed at  $800\text{ }^\circ\text{C}$ .

Figure 9 presents the effect of energy used for excitation on the NIR emission spectrum of the same  $\text{GdVO}_4$ : 1%  $\text{Bi}^{3+}$ , 7%  $\text{Yb}^{3+}$  sample annealed at  $800\text{ }^\circ\text{C}$ . It can be seen that the intensity of  $\text{Yb}^{3+}$  emission changes significantly with the corresponding excitation wavelength. Upon direct excitation in the  $\text{Yb}^{3+}$  ion ( $\lambda_{\text{exc}} = 951\text{ nm}$ ), the intensity of emission with a maximum at  $984\text{ nm}$  is very weak due

to the poor absorption of the  $\text{Yb}^{3+}$  ions as it was shown in the inset of Figure 3, whereas upon indirect excitation at 266 nm in the  $(\text{O}^{2-}-\text{V}^{5+})$  CT state or at 330 nm in the  $(\text{Bi}^{3+}-\text{V}^{5+})$  CT state [12] an intensity of the  $\text{Yb}^{3+}$  emission is much higher. This can be explained by the effective energy transfer from the host and  $\text{Bi}^{3+}$  ions to  $\text{Yb}^{3+}$  ions and a strong absorption of the host in the near-UV range (see Figure 3): the intensity of  $\text{Yb}^{3+}$  emission is higher at 266 nm excitation than at 330 nm excitation. A difference in the emission intensity observed for  $\text{Yb}^{3+}$  ions depending on the excitation in a type of the CT state may be due to the fact that because of the concentration of  $[\text{VO}_4]^{3-}$  groups in the matrix the transfer is much more probable than via  $\text{Bi}^{3+}$  ions, which play the role as a co-dopant.

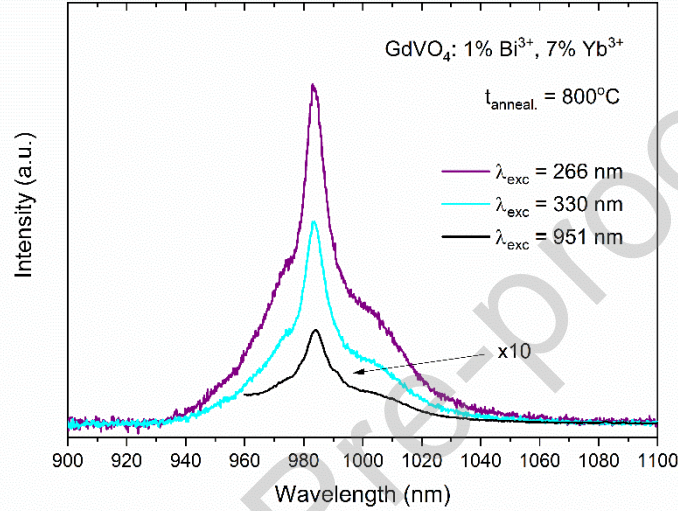


**Figure 9.** Impact of excitation wavelength on NIR emission spectra of the  $\text{GdVO}_4: 1\% \text{Bi}^{3+}, 7\% \text{Yb}^{3+}$  annealed at  $800^\circ\text{C}$  upon  $\lambda_{\text{exc}} = 266 \text{ nm}$  in the  $(\text{O}^{2-}-\text{V}^{5+})$  CT state,  $\lambda_{\text{exc}} = 330 \text{ nm}$  in the  $(\text{Bi}^{3+}-\text{V}^{5+})$  CT and  $\lambda_{\text{exc}} = 951 \text{ nm}$  in the  $\text{Yb}^{3+}$  ion, respectively.

In order to characterize the energy transfer processes occurring in the studied material, we focused on the analysis of these processes when the samples were excited with two wavelengths: (1) 266 nm in the  $(\text{O}^{2-}-\text{V}^{5+})$  CT state and (2) 330 nm in the  $(\text{Bi}^{3+}-\text{V}^{5+})$  CT state. Upon 266 nm excitation, the  $[\text{VO}_4]^{3-}$  groups are excited in the host matrix which next can transfer the energy directly to  $\text{Yb}^{3+}$  ions and also to  $\text{Bi}^{3+}$  ions, which was confirmed by Wei et al. in the work on  $\text{GdVO}_4: \text{Yb}^{3+}$  [38] by the presence of the  $(\text{O}^{2-}-\text{V}^{5+})$  CT band in the excitation spectrum for  $\text{Yb}^{3+}$  ions and in Figure 6 in this work in the case of excitation spectrum for  $\text{Bi}^{3+}$  ions. Energy transfer between the  $[\text{VO}_4]^{3-}$  groups and  $\text{Bi}^{3+}$  ions occurs through a thermally assisted migration process what was described by Moncorgé et al. [39] and Cavalli et al. [19]. Whereas, energy transfer from the host to the  $\text{Yb}^{3+}$  ions can occur theoretically in two ways: (1) through downconversion process owing to the absence of the energy overlap between the vanadate groups emission and absorption of  $\text{Yb}^{3+}$  ion and resonance between the energy of vanadate groups emission and the sum of the energy of absorption of two  $\text{Yb}^{3+}$  ions [40] and (2) as a phonon-assisted energy transfer from excited  $[\text{VO}_4]^{3-}$  groups to  $(\text{O}^{2-}-\text{Yb}^{3+})$  charge transfer state (CTS) [41]. In order to establish what mechanism of  $\text{Yb}^{3+}$  emission takes place in studied material, we have measured the power dependence of  $\text{Yb}^{3+}$  emission first. We have monitored the power dependence NIR emission intensities  ${}^2\text{F}_{5/2} \rightarrow {}^2\text{F}_{7/2}$  transition of  $\text{Yb}^{3+}$  ion upon excitation with a 266 nm diode laser source. In general, the emission intensity  $I$  varies with  $N$ th order of the incident pump power  $P$  as  $I \propto P^N$ . This dependence is classically described by  $N$  photon power-law  $P^N$ , where  $N$  is the order parameter determined by the slope of the log-log plot [42]. The dual-logarithmic plots for the integrated emission intensity versus pump power for  ${}^2\text{F}_{5/2} \rightarrow {}^2\text{F}_{7/2}$  transition in the  $1\% \text{Bi}^{3+}/(1\%, 5\%,$

7%)Yb<sup>3+</sup> co-doped gadolinium vanadate phosphor upon 266 nm excitation are shown in Figure 10. The slope values were found to be 1.20, 1.35 and 1.47 for samples with 1%, 5% and 7% Yb<sup>3+</sup>, respectively. Assuming two photon cutting for downconversion process  $[\text{VO}_4]^{3-} \rightarrow 2(\text{Yb}^{3+})^*$  the slope should be close to 1/2, as R. V. Yadav has recorded in Bi<sup>3+</sup>/Yb<sup>3+</sup> co-doped gadolinium tungstate phosphor [43]. This suggests that the NIR emission of Yb<sup>3+</sup> ions in this compound is rather a linear process. Since the GdVO<sub>4</sub> powder compound has high phonon energy (882 cm<sup>-1</sup>) and evident overlap of bands in Raman spectrum with Yb<sup>3+</sup> absorption below 200 cm<sup>-1</sup> is seen, it is more probable that a phonon-assisted energy transfer occurs in studied material. However, the order parameter  $N$  is significantly larger than 1 and increases with the content of Yb<sup>3+</sup> ions. It means that the energy transfer process between  $[\text{VO}_4]^{3-}$  groups and Yb<sup>3+</sup> ions is not solely a one-photon process. In his work J. Zhao has observed that character of energy transfer process changes depending on concentration of Yb<sup>3+</sup> ions [44]. For low concentration of Yb<sup>3+</sup> ions the energy transfer process from  $[\text{VO}_4]^{3-}$  groups to Yb<sup>3+</sup> ions is dominated by the single photon energy transfer but for higher concentration of Yb<sup>3+</sup> ions – above 0.08 in Ba<sub>2</sub>LaV<sub>3</sub>O<sub>11</sub> host [44], the downconversion process occurs, and its possibility gradually rises with the increase of Yb<sup>3+</sup> concentration. The results from power dependence measurements in studied material in this work indicate a similar substantiation. In Bi<sup>3+</sup>/Yb<sup>3+</sup> co-doped GdVO<sub>4</sub> the emission of Yb<sup>3+</sup> ions observed upon 266 nm excitation comes mainly from the single photon energy transfer but with an increasing concentration of Yb<sup>3+</sup> ions, the downconversion process can occur. Taking account the type of energy transfer process that is dominant in this material upon excitation of 266 nm, i.e. a phonon-assisted energy transfer, the course of this process should be considered, which results in NIR emission of Yb<sup>3+</sup> ions. Generally, NIR luminescence of Yb<sup>3+</sup> ion can be excited in different ways: (1) by direct excitation of  $^2\text{F}_{7/2} \rightarrow ^2\text{F}_{5/2}$  transition in Yb<sup>3+</sup> ion; (2) by nonradiative relaxation of the (O<sup>2-</sup>-Yb<sup>3+</sup>) CT state; (3) by radiative transition CTS  $\rightarrow ^2\text{F}_{5/2}$ , or by (4) impact excitation by hot electrons or holes [45]. The first and fourth way does not take place because the Yb<sup>3+</sup> ions are not excited directly, nor the electrons in the valence band. The third way does not take place either, because the emission from the (O<sup>2-</sup>-Yb<sup>3+</sup>) CT state is not observed in studied material, as is in the case of the YPO<sub>4</sub>: Yb<sup>3+</sup> [46]. Therefore, only the second way remains, via the nonradiative relaxation of the (O<sup>2-</sup>-Yb<sup>3+</sup>) CT state, similar to the case of Yb<sup>3+</sup> singly doped tellurite glasses [47]. In turn, the occurrence of downconversion process in the Bi<sup>3+</sup>/Yb<sup>3+</sup> co-doped GdVO<sub>4</sub> compound can more dominate at low temperatures – below 200 K at 266 nm excitation, what Jiang et al. has reported in Bi<sup>3+</sup>, Yb<sup>3+</sup> co-doped YVO<sub>4</sub> phosphor [48], which is due to a low efficiency phonon-assisted energy transfer in low temperature.

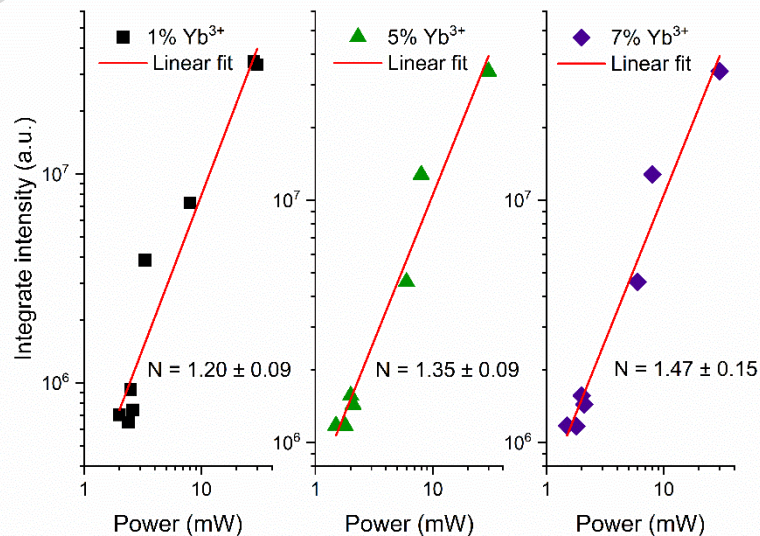


**Figure 10.** Power dependence of  $\text{Yb}^{3+}$  emission of the system  $\text{GdVO}_4$ : 1%  $\text{Bi}^{3+}$ , x%  $\text{Yb}^{3+}$  ( $x = 1, 5, 7$ ) excited by 266 nm.

In the case of direct excitation in the  $(\text{Bi}^{3+}-\text{V}^{5+})$  CT state ( $\lambda_{\text{exc}} = 330$  nm), the excited  $\text{Bi}^{3+}$  ions emit the light in the visible range and can transfer a part of their energy to the excited states of  $\text{Yb}^{3+}$  ions, what is manifested by a decrease in the intensity of the  $\text{Bi}^{3+}$  emission band in the  $\text{Bi}^{3+}/\text{Yb}^{3+}$  co-doped  $\text{GdVO}_4$  system (see Figure 7). That is why two types of emission (visible and infrared) are observed at the same time. This energy transfer occurs despite the lack of the energy overlap between the  $\text{Bi}^{3+}$  emission band and the absorption band of  $\text{Yb}^{3+}$  ions or  $(\text{O}^{2-}-\text{Yb}^{3+})$  CT state. Due to the fact that resonance between the energy of  $\text{Bi}^{3+}$  emission and the sum of the energy of absorption of two  $\text{Yb}^{3+}$  ions is possible, a downconversion process can be also between  $\text{Bi}^{3+}$  and  $\text{Yb}^{3+}$  ions. An efficient transfer energy from excited  $\text{Bi}^{3+}$  ions to two neighboring  $\text{Yb}^{3+}$  ions by the downconversion process was reported in the  $\text{Gd}_2\text{O}_3$  [49,50] and  $\text{Y}_2\text{O}_3$  [51] hosts and Yadav et al. has recorded quantum cutting process in  $\text{Bi}^{3+}/\text{Yb}^{3+}$  co-doped gadolinium tungstate phosphor [43]. In this situation, it is likely that downconversion may also occur between  $\text{Bi}^{3+}$  and  $\text{Yb}^{3+}$  ions in the  $\text{GdVO}_4$  host so this mechanism can be considered as one of the likely relaxation channels but no direct evidence was found for it in this work. Therefore, for the studied  $\text{Bi}^{3+}/\text{Yb}^{3+}$  co-doped  $\text{GdVO}_4$  system, the following energy transfer processes model takes place, presented in the form of a schematic diagram in Figure 11. In this model, upon the excitation with UV light (266 nm), the  $[\text{VO}_4]^{3-}$  groups absorb UV photons and are excited from the ground state  $^1\text{A}_1$  to the higher excited state of  $^1\text{T}_2$ . The excited state of  $[\text{VO}_4]^{3-}$  group is split into two levels, the energy of higher level is close to the energy of  $(\text{O}^{2-}-\text{Yb}^{3+})$  CTS, which is located at a relatively high-energy region ( $\lambda < 250$  nm) [38]. With the help of the phonons, the excited  $[\text{VO}_4]^{3-}$  groups can transfer its energy to the  $\text{O}^{2-}-\text{Yb}^{3+}$  couple taking them to the excited charge transfer state, from which  $\text{Yb}^{3+}$  via nonradiative relaxation downs to the  $^2\text{F}_{5/2}$  state and follows emission a NIR photon around 1  $\mu\text{m}$  [41]. At the same time, the excited  $[\text{VO}_4]^{3-}$  groups relaxing to the lower excitation state of  $^1\text{T}_1$  can transfer its energy also to the  $\text{Bi}^{3+}$  ions and to excite their  $(\text{Bi}^{3+}-\text{V}^{5+})$  MMCT state, from which next  $\text{Bi}^{3+}$  ions relax down and emit a green photon or transferring its energy to one nearby  $\text{Yb}^{3+}$  ion probably with the help of the phonons, followed by one NIR photon emission. When excited with near-UV light (330 nm), the  $\text{Bi}^{3+}$  ions directly absorb near-UV photons [12,19] and are excited from the ground state  $^1\text{S}_0$  to the their  $(\text{Bi}^{3+}-\text{V}^{5+})$  MMCT state and then can relax down and emit a green photon or transfer their energy to one of the nearby  $\text{Yb}^{3+}$  ions. Due to the large overlap between the  $(\text{O}^{2-}-\text{V}^{5+})$  CT state of the host and the  $(\text{Bi}^{3+}-\text{V}^{5+})$  MMCT state of the  $\text{Bi}^{3+}$  ion, upon 330 nm excitation the  $[\text{VO}_4]^{3-}$  groups are also excited, so they also absorb part of this energy and can transfer it to the  $\text{Bi}^{3+}$  and  $f-f$  excited state of  $\text{Yb}^{3+}$  ions, but their contribution to the absorption of this near-UV energy is much smaller than at 266 nm excitation.

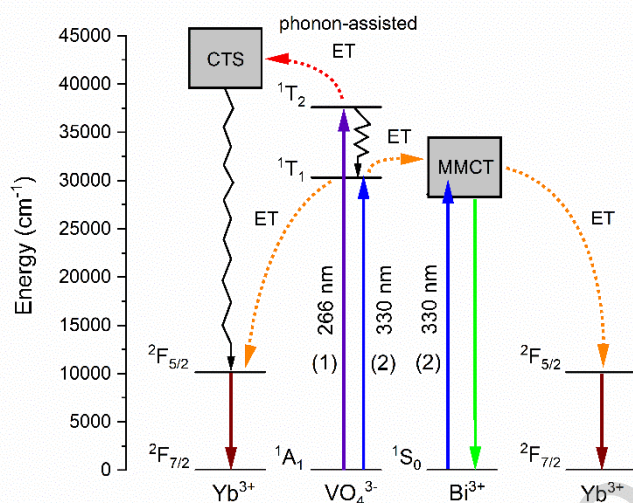


**Figure 11.** Schematic diagram of the  $[\text{VO}_4]^{3-}$ ,  $(\text{Bi}^{3+}\text{-V}^{5+})$  MMCT and  $\text{Yb}^{3+}$  energy levels and the energy transfer processes in the system  $\text{GdVO}_4: \text{Bi}^{3+}, \text{Yb}^{3+}$  upon excitation (1)  $\lambda_{\text{exc}} = 266 \text{ nm}$  and (2)  $\lambda_{\text{exc}} = 330 \text{ nm}$ , where CTS and ET refer to charge transfer state and energy transfer, respectively.

To gain a deeper insight into the energy transfer processes between  $\text{Bi}^{3+}$  and  $\text{Yb}^{3+}$  ions, their decay curves at the room temperature were also recorded. Figure 12 shows the luminescence dynamic curves for the  $(\text{Bi}^{3+}\text{-V}^{5+})$  CTS emission at 575 nm upon excitation  $\lambda_{\text{exc}} = 266 \text{ nm}$  with the different concentration of  $\text{Yb}^{3+}$  ions. The curves of the single doped  $\text{GdVO}_4: 1\% \text{ Bi}^{3+}$  and co-doped  $\text{GdVO}_4: 1\% \text{ Bi}^{3+}, 1\% \text{ Yb}^{3+}$  phosphors upon excitation  $\lambda_{\text{exc}} = 266 \text{ nm}$  show single exponential decay with the decay time of 3.65  $\mu\text{s}$  and 3.45  $\mu\text{s}$ , respectively. At a higher concentration of  $\text{Yb}^{3+}$  (5% and 7%), the decays are no longer single exponential curves and they show here the ongoing and more effective energy transfer process [49,52]. The decay time for samples co-doped with 5% and 7% of  $\text{Yb}^{3+}$  only for the longer component is shown in the Supplementary Material – Table S1. The values of the  $\text{Bi}^{3+}$  decay times obtained are similar to those recorded for a similar concentration range of co-dopants in  $\text{YVO}_4: \text{Bi}^{3+}, \text{Yb}^{3+}$  [48] or even  $\text{YVO}_4: \text{Bi}^{3+}, \text{Eu}^{3+}$  [53] upon excitation  $\lambda_{\text{exc}} = 266 \text{ nm}$  and  $\lambda_{\text{exc}} = 330 \text{ nm}$ , respectively. The single exponential character of the decay curves for the sample without  $\text{Yb}^{3+}$  and doped with 1%  $\text{Yb}^{3+}$  means the existence of only one relaxation process, which indicates that each  $\text{Bi}^{3+}$  donor ion has a similar distribution of  $\text{Yb}^{3+}$  acceptor ions around it. As the  $\text{Yb}^{3+}$  concentration increases, the homogeneous distribution of  $\text{Yb}^{3+}$  acceptor ions around each  $\text{Bi}^{3+}$  donor is disturbed, resulting in a non-exponential decay as well as a decrease in the  $\text{Bi}^{3+}$  lifetime. The introduction of the  $\text{Yb}^{3+}$  dopant creates extra decay pathways of  $\text{Bi}^{3+}$  emission due to the energy transfer to  $\text{Yb}^{3+}$ , which enhances the  $\text{Bi}^{3+}$  decay rate. These results strongly confirm the existence of energy transfer from  $\text{Bi}^{3+}$  to  $\text{Yb}^{3+}$  in the  $\text{GdVO}_4$  host. Additionally, the excitation in the  $(\text{O}^{2-}\text{-V}^{5+})$  CT state at 266 nm or direct in  $\text{Bi}^{3+}$  ions at 330 nm does not noticeably affect the  $\text{Bi}^{3+}$  emission decay time (as shown in the Supplementary Material – Table S1).

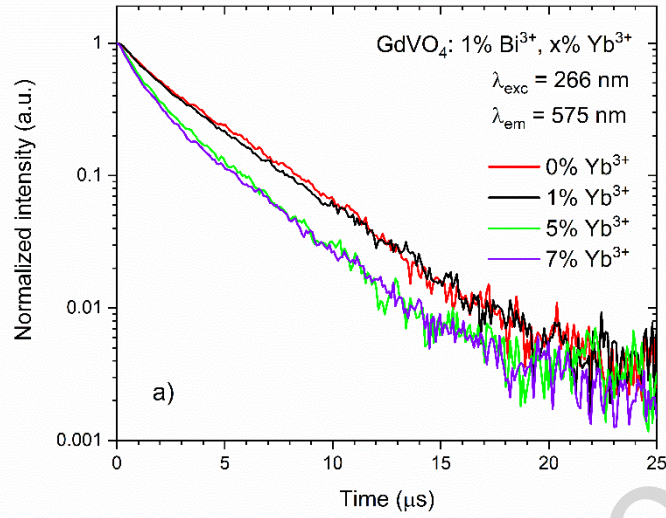


**Figure 12.** Decay curves of the ( $\text{Bi}^{3+}\text{-V}^{5+}$ ) CTS emission at 575 nm upon excitation  $\lambda_{\text{exc}} = 266$  nm for various concentration of  $\text{Yb}^{3+}$  ions in  $\text{GdVO}_4$ : 1%  $\text{Bi}^{3+}$ ,  $x\%$   $\text{Yb}^{3+}$  ( $x = 0, 1, 5, 7$ ).

Based on Förster-Dexter theory on energy transfer and taking into account that only one energy transfer channel is operative, the probability and efficiency of energy transfer from the  $\text{Bi}^{3+}$  donor to the  $\text{Yb}^{3+}$  acceptor ions can be characterized as follows [54]:

$$P_{\text{Bi-Yb}} = \frac{1}{\tau_D} \left( \frac{\eta_0}{\eta} - 1 \right) \quad (4)$$

$$\eta_{\text{Bi-Yb}} = 1 - \left( \frac{\eta}{\eta_0} \right) \quad (5)$$

where  $\eta_0$  and  $\eta$  are the fluorescence yield of the  $\text{Bi}^{3+}$  donor in the absence and presence of the  $\text{Yb}^{3+}$  acceptor ion,  $\tau_D$  is the decay constant of the pure  $\text{Bi}^{3+}$  donor. An alternative way to calculate the non-resonant energy transfer probability and efficiency based on the  $\text{Bi}^{3+}$  donor luminescence decay time in co-doped samples consists of adopting the relation [55]:

$$P_{\text{Bi-Yb}} = \left( \frac{1}{\tau} \right) - \left( \frac{1}{\tau_0} \right) \quad (6)$$

$$\eta_{\text{Bi-Yb}} = 1 - \left( \frac{\tau}{\tau_0} \right) \quad (7)$$

where  $\tau_0$  and  $\tau$  represent the lifetime of  $\text{Bi}^{3+}$  in the absence and presence of  $\text{Yb}^{3+}$ , respectively. All calculated results of  $P_{\text{Bi-Yb}}$  and  $\eta_{\text{Bi-Yb}}$  are shown in Figure 13. It was found that the probability and efficiency of the energy transfer from  $\text{Bi}^{3+}$  to  $\text{Yb}^{3+}$  increase with the  $\text{Yb}^{3+}$  concentration, which indicates a much more efficient energy transfer process occurring in the samples with higher  $\text{Yb}^{3+}$  ions concentration. The largest energy transfer efficiency from  $\text{Bi}^{3+}$  to  $\text{Yb}^{3+}$  is 29%. This is also a strong proof of the energy transfer from the  $\text{Bi}^{3+}$  to activators.

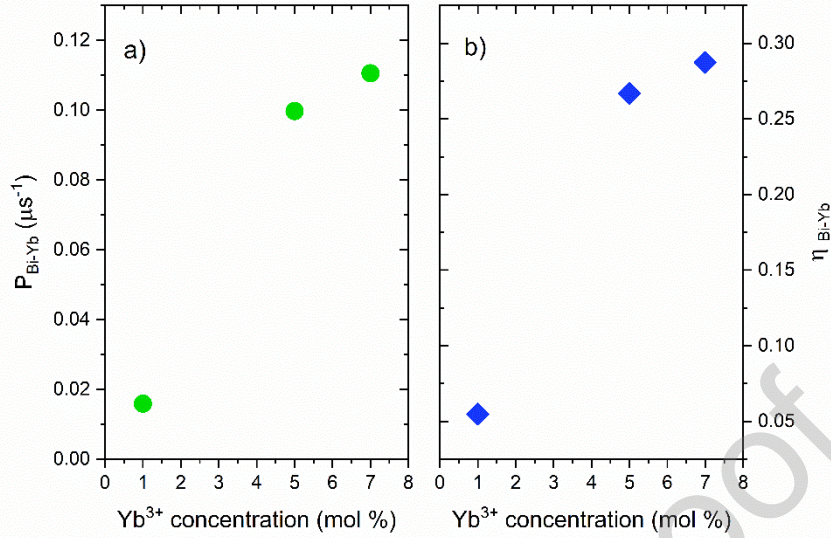


**Figure 13.** Dependence of the energy transfer probability  $P_{Bi-Yb}$  (a) and efficiency  $\eta_{Bi-Yb}$  (b) in GdVO<sub>4</sub>: 1% Bi<sup>3+</sup>, x% Yb<sup>3+</sup> (x = 0, 1, 5, 7) as a function of Yb<sup>3+</sup> doping concentration.

The decay curves for the Yb<sup>3+</sup> emission at 984 nm for different concentrations of Yb<sup>3+</sup> ions upon excitation  $\lambda_{exc} = 266$  nm shown in Figure 14a also exhibit single exponential behavior for all the samples. The luminescence lifetimes ( $\tau$ ) for the <sup>2</sup>F<sub>5/2</sub> state were evaluated from a single exponential fit and are shown in Figure 14b. It is observed that the lifetime does not change substantially with increasing the Yb<sup>3+</sup> concentration. The lack of the observed significant reduction of the Yb<sup>3+</sup> lifetime for higher concentrations of Yb<sup>3+</sup> ions in the sample indicates, therefore, no occurrence of a concentration quenching in the studied material when doped with Yb<sup>3+</sup> ions in the range of 0 - 7%, compared to the Bi<sup>3+</sup> and Yb<sup>3+</sup>-doped Y<sub>2</sub>O<sub>3</sub> host [41]. The obtained values of the Yb<sup>3+</sup> lifetimes are similar to those recorded for a similar concentration range of co-dopants in YVO<sub>4</sub>: Bi<sup>3+</sup>, Yb<sup>3+</sup> [48] upon excitation  $\lambda_{exc} = 266$  nm. Here, too, the excitation in the (O<sup>2-</sup>-V<sup>5+</sup>) CT state at 266 nm or in the Bi<sup>3+</sup> ions at 330 nm or directly in the Yb<sup>3+</sup> ions at 951 nm, does not noticeably affect the Yb<sup>3+</sup> emission lifetime (Supplementary Material – Table S2).

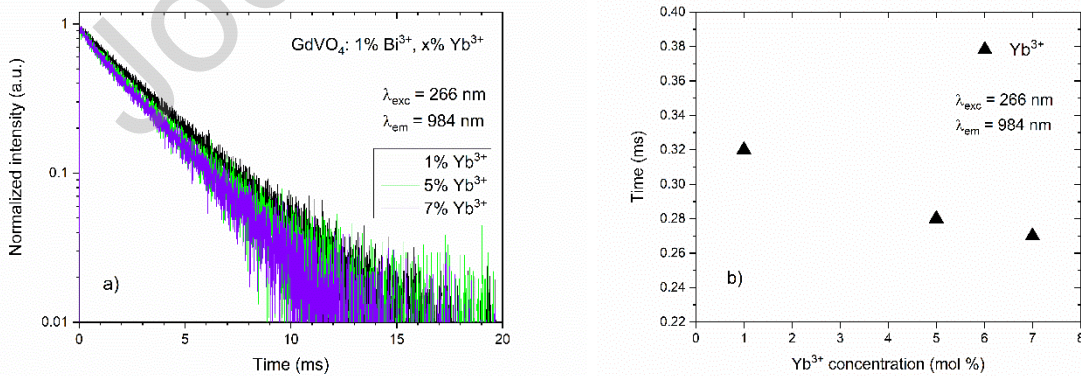


**Figure 14.** Decay curves of the <sup>2</sup>F<sub>5/2</sub> level of Yb<sup>3+</sup> emission at 984 nm (a) and lifetime of Yb<sup>3+</sup> (b) upon excitation  $\lambda_{exc} = 266$  nm for various concentration of Yb<sup>3+</sup> ions in GdVO<sub>4</sub>: 1% Bi<sup>3+</sup>, x% Yb<sup>3+</sup> (x = 0, 1, 5, 7).

#### 4. Conclusions

A structure, morphology, luminescence properties and energy transfer mechanisms of GdVO<sub>4</sub> co-doped with Bi<sup>3+</sup> and Yb<sup>3+</sup> ions obtained by the microwave-assisted hydrothermal synthesis method have been studied. The co-doped GdVO<sub>4</sub> material has a strong host absorption (O<sup>2-</sup>-V<sup>5+</sup>) CT band and the (Bi<sup>3+</sup>-V<sup>5+</sup>) CT absorption band in comparison to the absorption of Yb<sup>3+</sup> ions, which allows for the excitation of dopant ions indirectly. Recorded Raman spectrum for studied material has showed that the absorption spectrum has a vibrational nature caused by electron-phonon coupling. Furthermore, the electron-vibronic excitation spectrum does not essentially depend on the concentration of Yb<sup>3+</sup> and the size of the crystallites.

Observation of the CT bands in PLE spectrum, when monitoring the emission from Yb<sup>3+</sup> ions at 984 nm, demonstrates the involvement of the host and Bi<sup>3+</sup> ions in the generation of the Yb<sup>3+</sup> emission. Upon near-UV excitation Bi<sup>3+</sup> and Yb<sup>3+</sup> ions, the co-doped GdVO<sub>4</sub> shows an intense yellow-green emission coming from the Bi<sup>3+</sup> ions and the near infrared emission from the Yb<sup>3+</sup> ions, simultaneously, as an effect of energy transfer from the host and Bi<sup>3+</sup> ions to the Yb<sup>3+</sup> ions. Additionally, upon the indirect excitation, an intensity of the Yb<sup>3+</sup> emission is much higher than upon direct excitation in Yb<sup>3+</sup> ions.

The mechanism of energy transfer process in the GdVO<sub>4</sub> co-doped with Bi<sup>3+</sup>/Yb<sup>3+</sup> ions depends on concentration of Yb<sup>3+</sup> ions. For a low concentration of Yb<sup>3+</sup> ions the emission of Yb<sup>3+</sup> ions observed upon 266 nm excitation is due to the phonon-assisted energy transfer from the excited [VO<sub>4</sub>]<sup>3-</sup> groups to the O<sup>2-</sup>-Yb<sup>3+</sup> charge transfer state and then, by nonradiative relaxation to the *f-f* excited state of Yb<sup>3+</sup> ions. In case of higher concentration of Yb<sup>3+</sup> ions, a downconversion process can occur. In turn upon 330 nm excitation, the phonon-assisted energy transfer or downconversion may occur between Bi<sup>3+</sup> and Yb<sup>3+</sup> due to no energy overlap between the Bi<sup>3+</sup> emission band and the absorption band of Yb<sup>3+</sup> ions. The energy transfer efficiency from Bi<sup>3+</sup> to Yb<sup>3+</sup> at the highest Yb<sup>3+</sup> concentration (7 mol%) is 29% (no evidence of the luminescence concentration quenching of Yb<sup>3+</sup> ions in the range of 1 - 7 mol% has been noticed). The Bi<sup>3+</sup>/Yb<sup>3+</sup> co-doped GdVO<sub>4</sub> producing a NIR photon around 1 μm in a phonon-assisted ET process, offers the possibility of improving the spectral response of the silicon solar cells to short-wavelength sunlight.

**Acknowledgments:** The authors are very thankful to Mrs. Ewa Bukowska for X-ray powder diffraction measurements, to Mr. Robert Kowalski for fluorescence decay time measurements by using a femtosecond laser, to Dr. Robert Tomala for help in emission measurements in excitation power dependence and Dr. Radosław Lisiecki for help in in the analysis of emission and excitation spectra.

#### References

- [1] S. Asahi, H. Teranishi, K. Kusaki, T. Kaizu, T. Kita, Two-step photon up-conversion solar cells, *Nat. Commun.* 8 (2017) 1–9. <https://doi.org/10.1038/ncomms14962>.
- [2] H. Lian, Z. Hou, M. Shang, D. Geng, Y. Zhang, J. Lin, Rare earth ions doped phosphors for improving efficiencies of solar cells, *Energy*. 57 (2013) 270–283. <https://doi.org/10.1016/j.energy.2013.05.019>.
- [3] P. Moraitis, R.E.I. Schropp, W.G.J.H.M. van Sark, Nanoparticles for Luminescent Solar Concentrators - A review, *Opt. Mater. (Amst)*. 84 (2018) 636–645. <https://doi.org/10.1016/j.optmat.2018.07.034>.
- [4] L. Yang, S. Peng, M. Zhao, L. Yu, New synthetic strategies for luminescent YVO<sub>4</sub>:Ln<sup>3+</sup> (Ln = Pr, Sm, Eu, Tb, Dy, Ho, Er) with mesoporous cell-like nanostructure, *Opt. Mater. Express*. 8 (2018) 3805. <https://doi.org/10.1364/ome.8.003805>.
- [5] T. Samanta, A.E. Praveen, V. Mahalingam, Host sensitized intense infrared emissions from

- Ln<sup>3+</sup> doped GdVO<sub>4</sub> nanocrystals: ranging from 950 nm to 2000 nm, *J. Mater. Chem. C.* 6 (2018) 4878–4886. <https://doi.org/10.1039/c8tc00841h>.
- [6] K. Lenczewska, Y. Gerasymchuk, N. Vu, N.Q. Liem, G. Boulon, D. Hreniak, The size effect on the energy transfer in Bi<sup>3+</sup>–Eu<sup>3+</sup> co-doped GdVO<sub>4</sub> nanocrystals, *J. Mater. Chem. C.* 5 (2017) 3014–3023. <https://doi.org/10.1039/C6TC04660F>.
- [7] H. Luo, S. Zhang, Z. Mu, F. Wu, Z. Nie, D. Zhu, X. Feng, Q. Zhang, Near-infrared quantum cutting via energy transfer in Bi<sup>3+</sup>, Yb<sup>3+</sup> co-doped Lu<sub>2</sub>GeO<sub>5</sub> down-converting phosphor, *J. Alloys Compd.* 784 (2019) 611–619. <https://doi.org/10.1016/j.jallcom.2019.01.060>.
- [8] A.S. Vanetsev, O.M. Gaitko, I.G. Chuvashova, M.N. Sokolov, Y.D. Tret'yakov, Microwave hydrothermal synthesis of nanodispersed YV<sub>1-x</sub>P<sub>x</sub>O<sub>4</sub>:Eu powders, *Dokl. Chem.* 441 (2011) 325–329. <https://doi.org/10.1134/S0012500811110097>.
- [9] K. Lenczewska, R. Tomala, D. Hreniak, Near-UV sensitized NIR emission in Nd<sup>3+</sup> and Bi<sup>3+</sup> co-doped GdVO<sub>4</sub> phosphors, *Opt. Mater. (Amst).* 74 (2017) 12–15. <https://doi.org/10.1016/j.optmat.2017.04.015>.
- [10] K. Lenczewska, Y. Gerasymchuk, N. Vu, N.Q. Liem, G. Boulon, D. Hreniak, The size effect on the energy transfer in Bi<sup>3+</sup>–Eu<sup>3+</sup> co-doped GdVO<sub>4</sub> nanocrystals, *J. Mater. Chem. C.* 5 (2017) 3014–3023. <https://doi.org/10.1039/C6TC04660F>.
- [11] V.P. Gapontsev, A.A. Izyneev, Y.E. Sverchkov, M.R. Syrtlanov, MECHANISM AND PARAMETERS OF THE QUENCHING OF LUMINESCENCE OF RARE-EARTH IONS BY HYDROXYL IMPURITY GROUPS IN LASER PHOSPHATE GLASS., *Sov. J. Quantum Electron.* 8 (1981) 1101–1103. <https://doi.org/10.1070/qe1981v011n08abeh008063>.
- [12] K. Lenczewska, M. Stefanski, D. Hreniak, Synthesis, structure and NIR luminescence properties of Yb<sup>3+</sup> and Bi<sup>3+</sup>-activated vanadate GdVO<sub>4</sub>, *J. Rare Earths.* 34 (2016) 837–842. [https://doi.org/10.1016/S1002-0721\(16\)60103-5](https://doi.org/10.1016/S1002-0721(16)60103-5).
- [13] L. Vasylechko, A. Tupys, V. Hreb, V. Tsiurma, I. Lutsiuk, Y. Zhydachevskyy, New mixed Y<sub>0.5</sub>R<sub>0.5</sub>VO<sub>4</sub> and RVO<sub>4</sub>:Bi materials: Synthesis, crystal structure and some luminescence properties, *Inorganics.* 6 (2018) 94. <https://doi.org/10.3390/inorganics6030094>.
- [14] P.M. Diehm, P. Ágoston, K. Albe, Size-dependent lattice expansion in nanoparticles: Reality or anomaly?, *ChemPhysChem.* 13 (2012) 2443–2454. <https://doi.org/10.1002/cphc.201200257>.
- [15] L. Yang, L. Li, M. Zhao, C. Fu, G. Li, Is there lattice contraction in multicomponent metal oxides? Case study for GdVO<sub>4</sub>:Eu<sup>3+</sup> nanoparticles, *Nanotechnology.* 24 (2013) 305701–305711. <https://doi.org/10.1088/0957-4484/24/30/305701>.
- [16] M.M. El-Okr, M.A. Salem, M.S. Salim, R.M. El-Okr, M. Ashoush, H.M. Talaat, Synthesis of cobalt ferrite nano-particles and their magnetic characterization, *J. Magn. Mater.* 323 (2011) 920–926. <https://doi.org/10.1016/j.jmmm.2010.11.069>.
- [17] L. Ratke, P.W.C.N.-B.; S.; U.C.L. (University C.L. Voorhees, Growth and coarsening : Ostwald ripening in materials processing, Springer, 2002. <https://doi.org/10.1007/978-3-662-04884-9>.
- [18] D. Chen, Y. Yu, P. Huang, H. Lin, Z. Shan, L. Zeng, A. Yang, Y. Wang, Color-tunable luminescence for Bi<sup>3+</sup>/Ln<sup>3+</sup>:YVO<sub>4</sub> (Ln = Eu, Sm, Dy, Ho) nanophosphors excitable by near-ultraviolet light., *Phys. Chem. Chem. Phys.* 12 (2010) 7775–8. <https://doi.org/10.1039/c003678a>.
- [19] E. Cavalli, F. Angiuli, F. Mezzadri, M. Trevisani, M. Bettinelli, P. Boutinaud, M.G. Brik, Tunable luminescence of Bi<sup>3+</sup>-doped YPXV<sub>1-X</sub>O<sub>4</sub> (0 ≤ X ≤ 1), *J. Phys. Condens. Matter.* 26 (2014) 385503. <https://doi.org/10.1088/0953-8984/26/38/385503>.

- [20] A. Wu, S. Pan, J. Xu, T. Ogawa, S. Wada, M. Higuchi, K. Kodaira, Spectral properties of Yb:GdVO<sub>4</sub> crystals, *J. Cryst. Growth*. 311 (2009) 888–891. <https://doi.org/10.1016/j.jcrysgro.2008.09.171>.
- [21] Z.D.-C. Yi Juan, Qiu Jian-Bei, Wang Yu-An, Preparation and characterization of nanosized Gd<sub>x</sub>Bi<sub>0.95-x</sub>VO<sub>4</sub>:0.05Eu<sup>3+</sup> solid solution as red phosphor, *Chin. Phys. B*. 23 (2014) 104224–104230. <https://doi.org/10.1088/1674-1056/23/10/104224>.
- [22] F. Kang, H. Zhang, L. Wondraczek, X. Yang, Y. Zhang, D.Y. Lei, M. Peng, Band-Gap Modulation in Single Bi<sup>3+</sup>-Doped Yttrium-Scandium-Niobium Vanadates for Color Tuning over the Whole Visible Spectrum, *Chem. Mater.* 28 (2016) 2692–2703. <https://doi.org/10.1021/acs.chemmater.6b00277>.
- [23] S. Tang, M. Huang, J. Wang, F. Yu, G. Shang, J. Wu, Hydrothermal synthesis and luminescence properties of GdVO<sub>4</sub>:Ln<sup>3+</sup> (Ln = Eu, Sm, Dy) phosphors, *J. Alloys Compd.* 513 (2012) 474–480. <https://doi.org/10.1016/j.jallcom.2011.10.093>.
- [24] Z.M. Fang, Q. Hong, Z.H. Zhou, S.J. Dai, W.Z. Weng, H.L. Wan, Oxidative dehydrogenation of propane over a series of low-temperature rare earth orthovanadate catalysts prepared by the nitrate method, *Catal. Letters*. 61 (1999) 39–44. <https://doi.org/10.1023/a:1019096116289>.
- [25] T. V. Gavrilović, D.J. Jovanović, V.M. Lojpur, V. Dordević, M.D. Dramićanin, Enhancement of luminescence emission from GdVO<sub>4</sub>:Er<sup>3+</sup>/Yb<sup>3+</sup> phosphor by Li<sup>+</sup> co-doping, *J. Solid State Chem.* 217 (2014) 92–98. <https://doi.org/10.1016/j.jssc.2014.05.009>.
- [26] P. Rafailov, D. Dimitrov, Y.F. Chen, C.S. Lee, J.Y. Juang, Symmetry of the optical phonons in LuVO<sub>4</sub>: A Raman study, *Crystals*. 10 (2020) 341. <https://doi.org/10.3390/cryst10050341>.
- [27] N. Zhang, J. Wang, X. Hu, H. Zhang, C.C. Santos, A.P. Ayala, I. Guedes, Phonons in isostructural (Nd,Yb):YxGd<sub>1-x</sub>(VO<sub>4</sub>) laser crystals: A Raman scattering study, *J. Solid State Chem.* 184 (2011) 905–910. <https://doi.org/10.1016/j.jssc.2011.02.018>.
- [28] Y.K. Voron'ko, A.A. Sobol', V.E. Shukshin, A.I. Zagumennyi, Y.D. Zavartsev, S.A. Kutovoï, Raman spectroscopic study of structural disordering in YVO<sub>4</sub>, GdVO<sub>4</sub>, and CaWO<sub>4</sub> Crystals, *Phys. Solid State*. 51 (2009) 1886–1893. <https://doi.org/10.1134/S1063783409090200>.
- [29] P.G. Zverev, The influence of temperature on Raman modes in YVO<sub>4</sub> and GdVO<sub>4</sub> crystals, *J. Phys. Conf. Ser.* 92 (2007) 012073. <https://doi.org/10.1088/1742-6596/92/1/012073>.
- [30] B.L. Hurley, S. Qiu, R.G. Buchheit, Raman Spectroscopy Characterization of Aqueous Vanadate Species Interaction with Aluminum Alloy 2024-T3 Surfaces, *J. Electrochem. Soc.* 158 (2011) C125. <https://doi.org/10.1149/1.3562557>.
- [31] P. Vilanova-Martínez, J. Hernández-Velasco, A.R. Landa-Cánovas, F. Agulló-Rueda, Laser heating induced phase changes of VO<sub>2</sub> crystals in air monitored by Raman spectroscopy, *J. Alloys Compd.* 661 (2016) 122–125. <https://doi.org/10.1016/j.jallcom.2015.11.174>.
- [32] A. Bensalah, Y. Guyot, M. Ito, A. Brenier, H. Sato, T. Fukuda, G. Boulon, Growth of Yb<sup>3+</sup>-doped YLiF<sub>4</sub> laser crystal by the Czochralski method. Attempt of Yb<sup>3+</sup> energy level assignment and estimation of the laser potentiality, *Opt. Mater. (Amst)*. 26 (2004) 375–383. <https://doi.org/10.1016/j.optmat.2003.09.015>.
- [33] M. Ito, G. Boulon, A. Bensalah, Y. Guyot, C. Goutaudier, H. Sato, Spectroscopic properties, concentration quenching, and prediction of infrared laser emission of Yb<sup>3+</sup>-doped KY<sub>3</sub>F<sub>10</sub> cubic crystal, *J. Opt. Soc. Am. B*. 24 (2007) 3023. <https://doi.org/10.1364/josab.24.003023>.
- [34] S. Jandl, Y. Lvesque, V. Nekvasil, M. Bettinelli, Crystal-field study of Yb<sup>3+</sup> doped LuVO<sub>4</sub>, *J. Appl. Phys.* 103 (2008) 4–8. <https://doi.org/10.1063/1.2937244>.
- [35] R. Lisiecki, G. Dominiak-Dzik, T. Łukasiewicz, W. Ryba-Romanowski, Infrared-to-visible

- conversion of radiation in YVO<sub>4</sub> crystals doped with Yb<sup>3+</sup> and Tm<sup>3+</sup> ions, *J. Mol. Struct.* 704 (2004) 323–327. <https://doi.org/10.1016/j.molstruc.2004.01.062>.
- [36] S. Campos, A. Denoyer, S. Jandl, B. Viana, D. Vivien, P. Loiseau, B. Ferrand, Spectroscopic studies of Yb<sup>3+</sup>-doped rare earth orthosilicate crystals, *J. Phys. Condens. Matter.* 16 (2004) 4579–4590. <https://doi.org/10.1088/0953-8984/16/25/015>.
- [37] J. Petit, P. Loiseau, P. Goldner, B. Viana, D. Vivien, B. Ferrand, Optical spectroscopy and laser oscillation in a high-power laser material: Yb:GdVO<sub>4</sub>, *Solid State Lasers and Amplifiers.* 5460 (2004) 132. <https://doi.org/10.1117/12.546501>.
- [38] X. Wei, Y. Liu, G. Jiang, Y. Chen, M. Yin, W. Xu, Energy transfer mechanisms in yb 3+-doped gdvo 4 near-infrared downconversion nanophosphor, *J. Nanosci. Nanotechnol.* 11 (2011) 9556–9561. <https://doi.org/10.1166/jnn.2011.5234>.
- [39] R. Moncorgé, G. Boulon, Investigations of the absorption and emission properties along with energy transfer in pure and Bi<sup>3+</sup> doped YVO<sub>4</sub>, *J. Lumin.* 18–19 (1979) 376–380. [https://doi.org/10.1016/0022-2313\(79\)90144-3](https://doi.org/10.1016/0022-2313(79)90144-3).
- [40] X. Cheng, L. Su, Y. Wang, X. Zhu, X. Wei, Y. Wang, Near-infrared quantum cutting in YVO<sub>4</sub>:Yb<sup>3+</sup>-thin-films via downconversion, *Opt. Mater. (Amst).* 34 (2012) 1102–1106. <https://doi.org/10.1016/j.optmat.2012.01.014>.
- [41] X. Wei, S. Huang, Y. Chen, C. Guo, M. Yin, W. Xu, Energy transfer mechanisms in Yb<sup>3+</sup>-doped YVO<sub>4</sub> near-infrared downconversion phosphor, *J. Appl. Phys.* 107 (2010) 103107. <https://doi.org/10.1063/1.3425794>.
- [42] R. Tomala, K. Grzeszkiewicz, D. Hreniak, W. Strek, Downconversion process in Yb<sup>3+</sup>-doped GdAG nanocrystals, *J. Lumin.* 193 (2018) 70–72. <https://doi.org/10.1016/j.jlumin.2017.06.038>.
- [43] R.V. Yadav, R.S. Yadav, A. Bahadur, A.K. Singh, S.B. Rai, Enhanced Quantum Cutting via Li<sup>+</sup> Doping from a Bi<sup>3+</sup>/Yb<sup>3+</sup>-Codoped Gadolinium Tungstate Phosphor, *Inorg. Chem.* 55 (2016) 10928–10935. <https://doi.org/10.1021/acs.inorgchem.6b01439>.
- [44] J. Zhao, C. Guo, T. Li, D. Song, X. Su, Near-infrared down-conversion and energy transfer mechanism in Yb<sup>3+</sup>-doped Ba<sub>2</sub>LaV<sub>3</sub>O<sub>11</sub> phosphors, *Phys. Chem. Chem. Phys.* 17 (2015) 26330–26337. <https://doi.org/10.1039/c5cp04115e>.
- [45] I.A. Kamenskikh, N. Guerassimova, C. Dujardin, N. Garnier, G. Ledoux, C. Pedrini, M. Kirm, A. Petrosyan, D. Spassky, Charge transfer fluorescence and f-f luminescence in ytterbium compounds, *Opt. Mater. (Amst).* 24 (2003) 267–274. [https://doi.org/10.1016/S0925-3467\(03\)00133-2](https://doi.org/10.1016/S0925-3467(03)00133-2).
- [46] G. Wang, L. Gao, H. Zhu, W. Zhou, Hydrothermal synthesis of blue-emitting YPO<sub>4</sub>:Yb<sup>3+</sup> nanophosphor, *Front. Mater. Sci.* 10 (2016) 197–202. <https://doi.org/10.1007/s11706-016-0340-1>.
- [47] Y. Wang, X. Zhou, J. Shen, X. Zhao, B. Wu, S. Jiang, L. Li, Broadband Near-Infrared Down-Shifting by Yb-O Charge-Transfer Band in Yb<sup>3+</sup> Singly Doped Tellurite Glasses, *J. Am. Ceram. Soc.* 99 (2016) 115–120. <https://doi.org/10.1111/jace.13959>.
- [48] G. Jiang, X. Wei, Y. Chen, M. Yin, Broadband downconversion in bi 3+, yb 3+-co-doped yvo 4 phosphor, *J. Nanosci. Nanotechnol.* 11 (2011) 9484–9488. <https://doi.org/10.1166/jnn.2011.5231>.
- [49] X.Y. Huang, Q.Y. Zhang, Near-infrared quantum cutting via cooperative energy transfer in Gd<sub>2</sub>O<sub>3</sub>: Bi<sup>3+</sup>, Yb<sup>3+</sup> phosphors, in: *J. Appl. Phys.*, 2010: p. 113526. <https://doi.org/10.1063/1.3354063>.
- [50] Y. Zhydachevskyy, V. Tsiumra, M. Baran, L. Lipińska, P. Sybilski, A. Suchocki, Quantum

- efficiency of the down-conversion process in Bi<sup>3+</sup>–Yb<sup>3+</sup> co-doped Gd<sub>2</sub>O<sub>3</sub>, *J. Lumin.* 196 (2018) 169–173. <https://doi.org/10.1016/j.jlumin.2017.12.042>.
- [51] X.T. Wei, J.B. Zhao, Y.H. Chen, M. Yin, Y. Li, Quantum cutting downconversion by cooperative energy transfer from Bi<sup>3+</sup> to Yb<sup>3+</sup> in Y<sub>2</sub>O<sub>3</sub> phosphor, *Chinese Phys. B.* 19 (2010) 077804. <https://doi.org/10.1088/1674-1056/19/7/077804>.
- [52] L. Wang, H. Guo, Y. Wei, H.M. Noh, J.H. Jeong, White luminescence and energy transfer process in Bi<sup>3+</sup>, Sm<sup>3+</sup> co-doped Ca<sub>3</sub>Al<sub>2</sub>O<sub>6</sub> phosphors, *Opt. Mater. (Amst).* 42 (2015) 233–236. <https://doi.org/10.1016/j.optmat.2014.12.037>.
- [53] J. Su, X. Mi, J. Sun, L. Yang, C. Hui, L. Lu, Z. Bai, X. Zhang, Tunable luminescence and energy transfer properties in YVO<sub>4</sub>:Bi<sup>3+</sup>, Eu<sup>3+</sup> phosphors, *J. Mater. Sci.* 52 (2017) 782–792. <https://doi.org/10.1007/s10853-016-0375-9>.
- [54] R. Reisfeld, E. Greenberg, R. Velapoldi, B. Barnett, Luminescence quantum efficiency of gd and tb in borate glasses\* and the mechanism of energy transfer between them, *J. Chem. Phys.* 56 (1972) 1698–1705. <https://doi.org/10.1063/1.1677427>.
- [55] A.D. Sontakke, K. Biswas, R. Sen, K. Annapurna, Efficient non-resonant energy transfer in Nd<sup>3+</sup>–Yb<sup>3+</sup> codoped Ba–Al–metaphosphate glasses, *J. Opt. Soc. Am. B.* 27 (2010) 2750. <https://doi.org/10.1364/josab.27.002750>.

**CRedit authorship contribution statement**

**Katarzyna Lenczewska:** Conceptualization, Methodology, Investigation, Validation, Formal analysis, Resources, Visualization, Writing - Original Draft, Writing - Review & Editing.

**Maciej Ptak:** Investigation (Raman measurement), Formal analysis, Validation.

**Vitalii Boiko:** Investigation (spectroscopic measurements), Validation.

**Karolina Ledwa:** Investigation (TEM images), Validation.

**Dariusz Hreniak:** Conceptualization, Methodology, Resources, Supervision, Writing - Review & Editing.

Journal Pre-proof

**Declaration of interests**

The authors declare that they have no known competing financial interests or personal relationships that could have appeared to influence the work reported in this paper.

The authors declare the following financial interests/personal relationships which may be considered as potential competing interests:

Journal Pre-proof

**Highlights:**

- 1)  $\text{GdVO}_4:\text{Bi}^{3+},\text{Yb}^{3+}$  phosphors were prepared by a microwave-assisted hydrothermal method.
- 2)  $\text{GdVO}_4:\text{Bi}^{3+},\text{Yb}^{3+}$  can be excited by broadband UV light and produce VIS and NIR emission.
- 3) A phonon-assisted energy transfer between the host,  $\text{Bi}^{3+}$  and  $\text{Yb}^{3+}$  ions was confirmed.

Journal Pre-proof

## Graphical abstract

